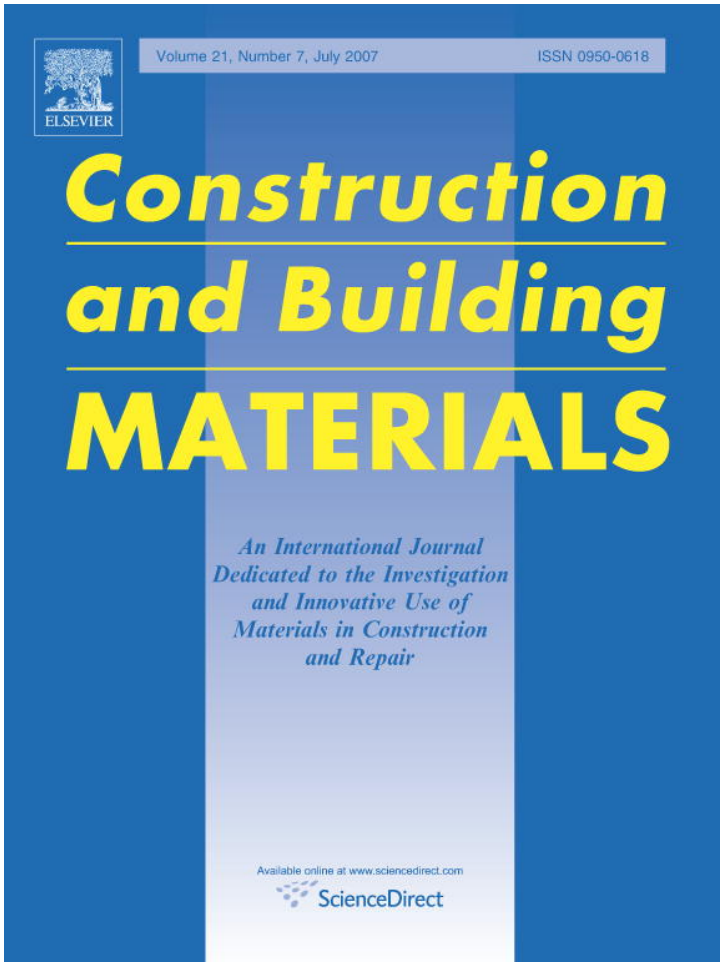

Available online at www.sciencedirect.com
ScienceDirect
Construction and Building Materials 21 (2007) 1415–1430
Construction and Building MATERIALS
www.elsevier.com/locate/conbuildmat

Reduction of the lateral thrust of masonry arches and vaults with FRP composites

Laura De Lorenzis *, Rossana Dimitri, Antonio La Tegola

Department of Innovation Engineering, University of Lecce, Via per Monteroni, 73100 Lecce, Italy

Received 15 March 2006; received in revised form 3 July 2006; accepted 14 July 2006
Available online 14 September 2006

Abstract

Fiber-reinforced polymer (FRP) composites are being increasingly used for rehabilitation and strengthening of masonry structures and, in particular, to strengthen masonry arches and vaults against their most critical failure mechanisms. The FRP reinforcement, introducing tension resistance, allows the line of thrust to fall outside the thickness of the arch. This fact has two important consequences: the capacity of the arch itself is increased, and the lateral thrust transmitted to the piers is reduced, thereby increasing the capacity of the "arch + piers" system. While the first effect has been stressed by existing research, less attention has been paid to the second effect, which nevertheless is very important for practical applications. In this paper, the effect of bonding an FRP sheet to the intrados of a circular arch on the minimum value of the lateral thrust is evaluated analytically. The model is then applied in particular to the four lateral arches of an edge vault. Edge vaults are a valuable part of the architectural and cultural heritage of some regions of Italy, and are structurally similar to cross-vaults except for the presence of a double-curvature shell portion in the middle of four barrel webs. These vaults are usually subjected to symmetric loading, as a result of the large dead-to-live load ratio. Hence, collapse of a vault typically occurs when no tie-rods or tie-beams are adopted and the piers are unable to bear the thrust of the vault. The paper also illustrates results of an experimental investigation on masonry edge vaults strengthened with FRP composites and subjected to uniform loading with measurement of the lateral thrust. Test results and theoretical predictions are presented and discussed.

Keywords: Arch; Fiber-reinforced polymer; Masonry; Thrust; Vault

1. Introduction

Masonry arches and vaults are often encountered in masonry buildings throughout Europe. Due to material degradation, imposed displacements, structural alterations induced by architectural changes, or increased service loads, these members often need repair and/or strengthening. For this purpose, fiber-reinforced polymer (FRP) composites in the form of externally bonded sheets applied to the surface of the arch or vault with the wet lay-up technique are an effective solution, as demonstrated by the available experimental and theoretical studies (e.g. [7,18,4,10,12]). In addition to being structurally effective, FRPs present several advantages over conventional techniques: they add no extra weight to the structure, are corrosion-resistant, have minimal aesthetic impact, and can be removed by raising the temperature above the glass transition temperature of the resin matrix. Minimal invasiveness and reversibility of the intervention are required in the strengthening of historic structures [13,14]. The available studies on strengthening of masonry vaults with FRP composites are relatively limited. The most comprehensive test program on vaults is that in Foraboschi [10], encompassing barrel, cross, and cloist vaults. Test results on barrel vaults have also been reported in Valluzzi et al. [18].

Analysis of masonry arches and vaults in the framework of limit analysis assumes that (i) masonry has no tensile strength and infinite compressive strength, and (ii) sliding

* Corresponding author.
E-mail address: laura.delorenzis@unile.it (L.De. Lorenzis).

0950-0618/$ - see front matter © 2006 Elsevier Ltd. All rights reserved.
doi:10.1016/j.conbuildmat.2006.07.009

failure does not occur [11]. The consequence of these assumptions is that failure of a masonry arch theoretically occurs by formation of a sufficient number of hinges transforming the arch into a mechanism, and stability under given loads depends essentially on the geometry of the structure. From the kinematic standpoint, the effect of the FRP composites is to inhibit the formation of the hinges. At a location where the FRP sheet is bonded, no hinge can open on the opposite side of the arch thickness. Depending on the extension and location of the strengthened portions of the arch and on the loading pattern, the formation of hinges may be either altered (i.e. hinges form at different locations than in the unstrengthened arch) or completely prevented. Therefore, the capacity of the arch may be controlled by local failure mechanisms depending on material properties, such as masonry crushing, sliding of mortar joints, and FRP debonding or rupture. From the static standpoint, the presence of the FRP reinforcement allows the line of thrust to fall outside the thickness of the arch by introducing tension resistance.

Most of the arches and vaults tested in the available studies were subjected to asymmetric loading so that failure of the unstrengthened arches or vaults occurred by formation of a mechanism involving the arch or vault itself and not involving the piers. In real structures, the degree of symmetry of the load pattern depends on the ratio of dead to live loads. In many cases, the dead load due to self weight and weight of the spandrel fill is significantly larger than the live load. Hence the loading condition of the arch or vault is approximately symmetric, and collapse often occurs when no tie-rods or tie-beams are adopted and the piers are unable to bear the thrust of the vault. In other words, the controlling failure mechanism of the arch or vault involves formation of three hinges plus spreading of the supports, as the alternative symmetric collapse mechanism (involving the formation of five hinges) typically corresponds to a larger load multiplier. In these cases, externally bonded FRP sheets can be used to reduce the lateral thrust transmitted by the vault to its piers, which is very important for practical applications. For new structures, it implies that FRP-reinforced arches may not need tie-rods or massive piers. For strengthening of existing structures, it indicates that bonding FRP sheets can be an effective measure when (as often happens) the deficiency of the structure depends on the inability of the piers to bear the lateral thrust and/or on the removal of tie-rods.

In this paper, the effect of bonding an FRP sheet to the intrados of a circular arch on the minimum value of the lateral thrust is first evaluated analytically. The effect of the amount of FRP on the lateral thrust is analyzed. The model is then applied, under appropriate simplifying assumptions, to the four lateral arches of an edge vault. Edge vaults are a valuable part of the architectural and cultural heritage of some regions of Italy (in particular of the Salento peninsula in southern Italy), and are structurally similar to cross-vaults except for the presence of a double-curvature shell portion in the middle of four barrel webs. These vaults are usually subjected to symmetric loading, as a result of the large dead-to-live load ratio. Hence, collapse of a vault typically occurs when no tie-rods or tie-beams are adopted and the piers are unable to bear the thrust of the vault. The available knowledge on the structural behaviour of this type of vaults is still very limited [6]. Within a wider research project on structural behaviour and failure modes of masonry structures, experimental tests were carried out on scaled prototypes of edge vaults, strengthened with FRP composites and subjected to uniform loading with measurement of the lateral thrust. Test results and theoretical predictions are presented and discussed in this paper.

2. Minimum lateral thrust of semicircular arches under uniform loading

2.1. Problem statement

The following analysis is conducted on a masonry arch with semicircular intrados and extrados of radii R_i and R_e, respectively, average radius of the arch $R = (R_i + R_e)/2$, span $L = 2R$. The arch has unit width, constant thickness $s = R_e - R_i$, and is loaded by its own weight (specific weight w) and a uniformly distributed load q. It is assumed that the arch is strengthened with FRP at the intrados, that the strengthened portion is symmetric about the y axis and spans a total angle 2α (Fig. 1).

Computation of the lateral thrust for the statically indeterminate arch is a complex task. At the same time, results are hardly meaningful [11], as phenomena such as small settlements, cracking, creep will significantly alter the state of the structure with time. However, the value of the lateral thrust ranges between a minimum and a maximum, which depend only on the geometry and the loading condition of the arch [11]. Moreover, the actual lateral thrust is usually closer to the minimum value [2]. Hence, this minimum value will be computed in the following. For the unstrengthened arch, the usual assumptions of limit analysis (recalled in the introduction) are maintained. For the strengthened arch, the compressive strength of masonry is

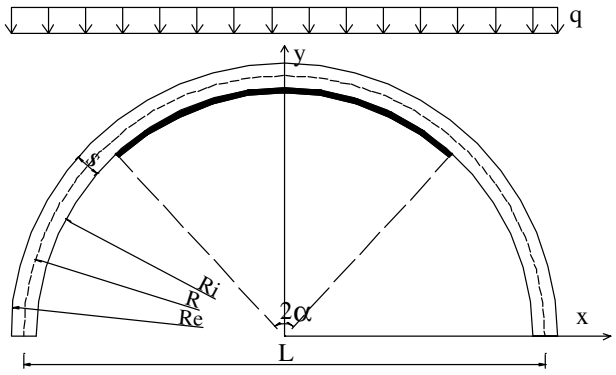

Fig. 1. Semicircular arch under uniform loading strengthened at the intrados with FRP.

considered finite but it is assumed that sliding failure does not occur. The latter assumption is verified afterwards.

Fig. 2 shows the scheme adopted for the computation of the minimum thrust for the unstrengthened arch (Fig. 2a, [3]) and for the arch strengthened at the intrados with FRP (Fig. 2b). The figure refers to half arch due to symmetry. A hinge is set in the intrados in a generic position D, defined by the angle θ (assuming the hinge is located on the intrados implies that the compressive strength of masonry is considered infinite for the unstrengthened portions of the arch, which does not introduce appreciable error). Due to symmetry and to equilibrium of forces, the internal force at the crown section is equal in magnitude and opposite in direction to the lateral thrust H_a. Equilibrium of moments of ABCD about D indicates that the minimum value of H_a is obtained when the distance of vector H_a from D is maximum. For the unstrengthened arch, this implies that H_a must be located at the extrados of the crown section, i.e. a hinge is assumed to form in B. In the strengthened arch, due to the presence of the FRP at the intrados, H_a is allowed to fall outside the thickness of the crown section (Fig. 2b). As no hinge can form at the extrados of the crown section, the limit condition for this section will correspond to failure under combined compression and bending. The maximum eccentricity e_u of H_a will thus depend on the material properties of masonry and FRP, on the reinforcement ratio of the crown section, and on the value of H_a itself.

2.2. Failure of an FRP-strengthened masonry section under compression and bending

The capacity of FRP-strengthened masonry sections under a compressive axial force N and a bending moment M can be determined based on the following assumptions: (a) plane cross-sections remain plane, (b) linear-elastic behaviour of the FRP in tension, (c) rectangular stress block for masonry in compression, with an equivalent depth of 0.8 times the neutral axis depth. As a consequence of these assumptions, the ultimate moment M_u of the cross-section subjected to a normal compressive force H_a can be easily computed [16,17,5] and is recalled as follows. The amount of reinforcement is expressed through the FRP normalized area fraction, given by

$$\omega = \frac{\varepsilon_{Mu} E_{frp}}{f_{Mu}} \frac{A_{frp}}{bs} \tag{1}$$

where ε_{Mu} is the ultimate strain of masonry in compression, E_{frp} and A_{frp} are the elastic modulus and the cross-sectional area of the FRP, respectively, f_{Mu} is the compressive strength of masonry, and b and s are the width and height of the cross-section, respectively (corresponding to the arch width and thickness).

Case (a): Failure of the FRP in tension

If $\omega \leqslant \omega_{lim}$, where:

$$\omega_{lim} = \frac{\varepsilon_{Mu}}{\varepsilon_{frpu}} \left[\frac{0.8}{1 + \frac{\varepsilon_{frpu}}{\varepsilon_{Mu}}} - \frac{N}{bsf_{Mu}} \right] \tag{2}$$

the FRP composite reaches its ultimate tensile strain before the maximum compressive strain of masonry reaches its ultimate value ε_{Mu}, hence the cross-section fails due to rupture of the FRP. In Eq. (2), ε_{frpu} is the FRP ultimate tensile strain and can possibly be multiplied by a reduction factor to account for FRP debonding prior to tensile rupture. Debonding is particularly likely when the FRP is applied at the intrados [18,1].

If $\omega \leqslant \omega_{lim}$, the ultimate moment is given by

$$M_u = bs^2 f_{Mu} \left[\frac{1}{2} \omega \frac{\varepsilon_{frpu}}{\varepsilon_{Mu}} + 0.4\bar{x}(1 - 0.8\bar{x}) \right] \tag{3}$$

where

$$\bar{x} = \frac{x}{s} = \frac{1}{0.8} \left[\frac{N}{bsf_{Mu}} + \omega \frac{\varepsilon_{frpu}}{\varepsilon_{Mu}} \right] \tag{4}$$

is the non-dimensional depth of the neutral axis at failure. Dividing Eq. (3) by N yields the maximum eccentricity of N, e_u. In particular, for the strengthened crown section of the arch, $N = H_a$ and hence its maximum eccentricity is

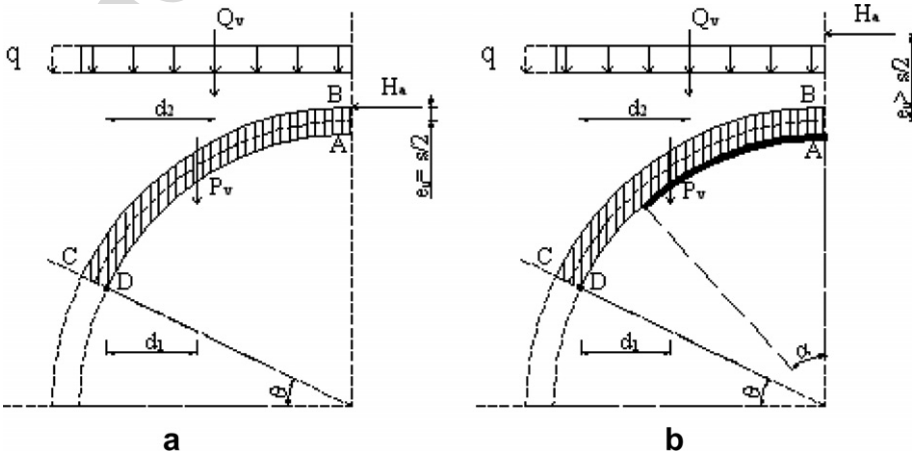

Fig. 2. Computation of minimum lateral thrust for the unstrengthened (a) and strengthened (b) arch under uniform loading.

$$e_u = s\frac{bsf_{Mu}}{H_a}\left[\frac{1}{2}\omega\frac{\varepsilon_{frpu}}{\varepsilon_{Mu}} + 0.4\bar{x}(1-0.8\bar{x})\right] \quad (5)$$

with $\bar{x}$ given by Eq. (4) with $N = H_a$.

Case (b): Failure of masonry in compression

If $\omega \geqslant \omega_{lim}$, failure occurs by crushing of masonry in compression. The ultimate moment is given by

$$M_u = bs^2 f_{Mu}\left[\frac{1}{2}\omega\frac{1-\bar{x}}{\bar{x}} + 0.4\bar{x}(1-0.8\bar{x})\right] \quad (6)$$

where:

$$\bar{x} = \frac{x}{s} = \frac{1}{1.6}\left[\frac{N}{bsf_{Mu}} - \omega + \sqrt{\left(\omega - \frac{N}{bsf_{Mu}}\right)^2 + 3.2\omega}\right] \quad (7)$$

is the non-dimensional depth of the neutral axis at failure. Dividing Eq. (6) by N yields the maximum eccentricity of N, e_u. In particular, for the strengthened crown section of the arch, $N = H_a$ and hence its maximum eccentricity is

$$e_u = s\frac{bsf_{Mu}}{H_a}\left[\frac{1}{2}\omega\frac{1-\bar{x}}{\bar{x}} + 0.4\bar{x}(1-0.8\bar{x})\right] \quad (8)$$

with $\bar{x}$ given by Eq. (7) with $N = H_a$. Eqs. (6)–(8) apply when the stress in the FRP is tensile, i.e. when $x/s < 1$. For $x/s \geqslant 1$ (i.e. for $N/bsf_{Mu} \geqslant 0.8$), the above equations may be replaced by ignoring the compressive strength of the FRP, i.e. setting $\omega = 0$ as follows:

$$M_u = bs^2 f_{Mu} 0.4\bar{x}(1-0.8\bar{x}) \quad (9)$$

$$\bar{x} = \frac{x}{s} = \frac{1}{0.8}\frac{N}{bsf_{Mu}} \quad (10)$$

$$e_u = s\frac{bsf_{Mu}}{N}0.4\bar{x}(1-0.8\bar{x}) \quad (11)$$

The equations above are valid for unstrengthened cross-sections as well. Figs. 3a and b show how M_u and e_u vary with N for different values of ω. In the figures, the $\varepsilon_{frpu}/\varepsilon_{Mu}$ ratio is taken equal to 3 (a lower bound value for the most common FRP properties). As a result, the cross-section is tension controlled only for the smallest considered amount of FRP ($\omega = 0.05$) and for the smallest values of axial force. The transition to compression-controlled failure is marked in Fig. 3a by the change in slope of the curve corresponding to $\omega = 0.05$ (indicated with the arrow). Fig. 3c also shows how the ultimate moment is affected by the amount of FRP for different values of axial force. The rate of increase of the ultimate moment with ω is large for small values of ω. However, for large amounts of FRP the ultimate moment becomes about constant, and the value it attains is larger for smaller values of the axial force.

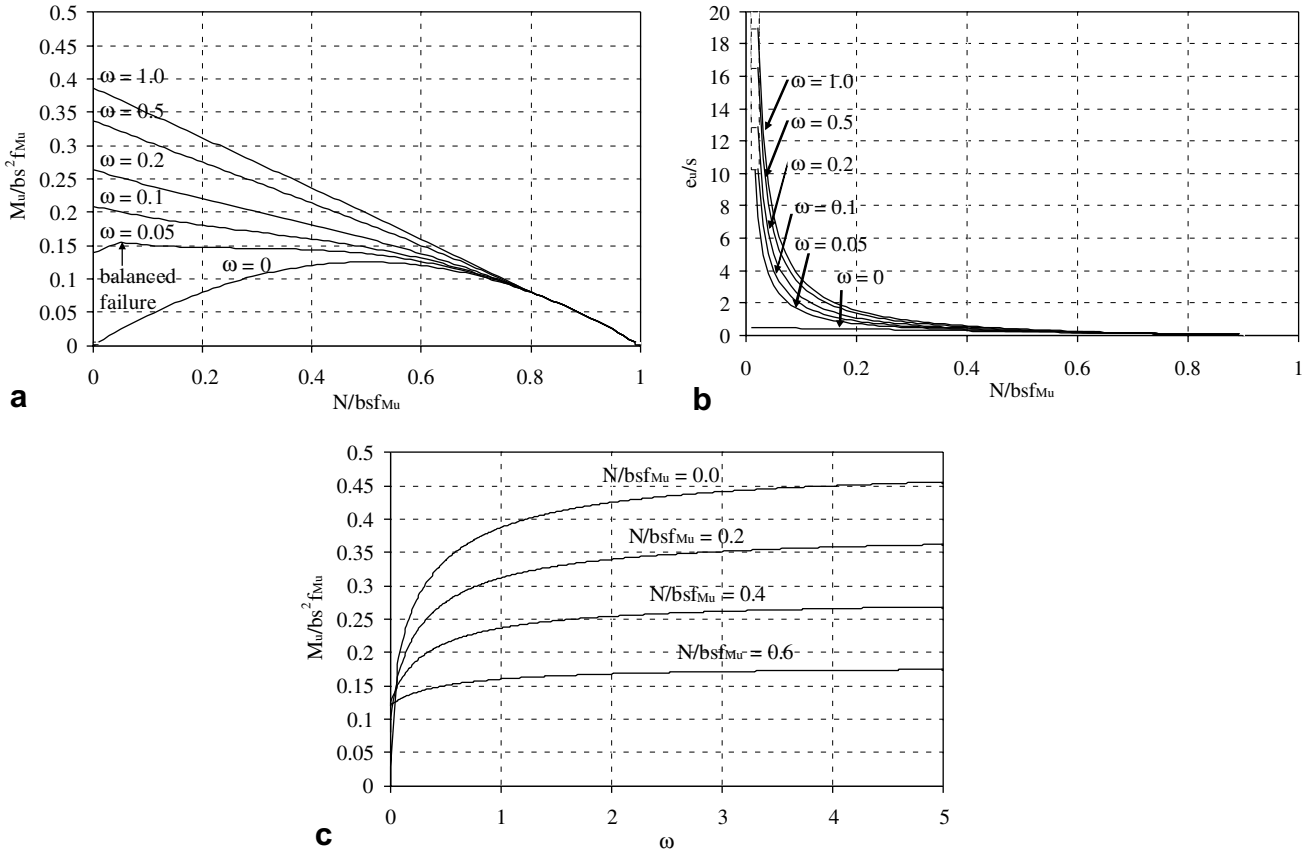

Fig. 3. Behavior of an FRP-strengthened masonry section under combined compression and bending. $\varepsilon_{frpu}/\varepsilon_{Mu} = 3$. (a) Normalized ultimate moment as a function of the normalized axial force for different FRP normalized area fractions. (b) Normalized ultimate eccentricity as a function of the normalized axial force for different FRP normalized area fractions. (c) Normalized ultimate moment as a function of the FRP normalized area fraction for different normalized axial forces.

2.3. Computation of the minimum lateral thrust

From equilibrium of moments of ABCD about D (Fig. 2):

$$H_a[R + e_u - R_i \sin\theta] = P_v d_1 + Q_v d_2 \quad (12)$$

where P_v is the self weight of ABCD, Q_v is the resultant of the distributed load acting on ABCD, and d_1 and d_2 are the respective distances from D. P_v, Q_v, d_1 and d_2 can be obtained from simple geometric considerations:

$$P_v = \frac{\pi}{2} wRs\left(1 - 2\frac{\theta}{\pi}\right); \quad d_1 = R_i \cos\theta - \frac{2R(1-\sin\theta)}{\pi\left(1 - 2\frac{\theta}{\pi}\right)} \quad (13a\text{-}b)$$

$$Q_v = qR_e \cos\theta; \quad d_2 = \left(R_i - \frac{R_e}{2}\right)\cos\theta \quad (14a\text{-}b)$$

For the unstrengthened arch, $e_u = s/2$ and H_a is immediately found from Eq. (12) as a function of θ. For the strengthened arch, e_u depends on H_a according to Eq. (5) or Eq. (8). Hence, for each value of θ, H_a must be found by solving Eq. (12) numerically.

2.4. Effect of FRP reinforcement ratio on the minimum lateral thrust

2.4.1. Example 1

In this example, the following geometry and material properties are assumed: $s = 700$ mm, $R = 5$ m (hence the span to thickness ratio of the arch is about 14), $f_{Mu} = 1$ N/mm^2, $\varepsilon_{Mu} = 0.003$, $E_{frp} = 200$ GPa, $\varepsilon_{frpu} = 0.01$. It is further assumed that $w = 18000$ N/m^3 and $q = 5000$ N/m^2. All computations are made per unit thickness of the arch.

Fig. 4a shows H_a as a function of θ for the unstrengthened arch. For θ ranging from 90° to about 60°, only one value of θ corresponds to a given H_a, indicating that the line of thrust intersects the intrados of the arch at one location. Tensile stresses at the extrados are necessary in the radial sections where the line of thrust is outside the thickness, which contradicts the assumption of masonry zero tensile strength. For θ lower than 60°, each value of H_a corresponds to two values of θ, i.e. the line of thrust intersects the intrados at two locations. Again tensile stresses at the extrados are necessary in the radial sections comprised between the two intersections. These two intersections get closer as H_a increases, and the maximum H_a corresponds to the tangency of the line of thrust to the intrados of the arch. This is the only condition compatible with the absence of tensile stresses in masonry. Hence the correct value of θ, θ_{min}, is the point of maximum of the curve, and the searched value of the thrust is the maximum H_a that can be obtained from Eq. (12). This is the minimum thrust of the arch, H_{amin}.

Fig. 4a also shows H_a as a function of θ for the arch strengthened at the intrados with different FRP normalized reinforcement ratios. For a given value of θ, H_a decreases with increasing ω, as a result of the larger eccentricity e_u allowed in the crown section. The same considerations made before for the unstrengthened arch apply to the strengthened arch: as the latter is only strengthened at the intrados, no tensile stresses at the extrados are allowed and the searched values of θ_{min} and H_{amin} correspond to the maximum of the curve, i.e. to the condition of tangency of the line of thrust to the intrados of the arch.

Note that, differently than in the unstrengthened case, for the strengthened arch the range of θ, for which a positive value of the corresponding thrust H_a can be calculated is less than 90°. This is easily explained by rewriting Eq. (12) as follows:

$$H_a[R - R_i \sin\theta] + M_u(H_a) = P_v d_1 + Q_v d_2 \quad (15)$$

For the strengthened arch, assuming $\omega \geqslant \omega_{lim}$ (in this example, ω_{lim} is 0.048), $M_u(H_a)$ increases as H_a decreases, reaching its maximum for $H_a = 0$ (Fig. 3). As θ increases, the second member of Eq. (15) (i.e. the moment about D of the external loads) decreases. If θ is large enough, no positive value of H_a is small enough to allow the first member of Eq. (15) (i.e. the moment about D of the internal forces) to equate the second. For a zero value of the thrust, Eq. (15) becomes:

$$M_{u0} = P_v(\theta_{lim}) d_1(\theta_{lim}) + Q_v(\theta_{lim}) d_2(\theta_{lim}) \quad (16)$$

where $M_{u0} = M_u(H_a = 0)$ is the ultimate moment of the strengthened cross-section under pure bending, and θ_{lim} is the maximum value of θ for which a positive thrust H_a can be computed. As visible from Fig. 4a, θ_{lim} decreases as the FRP reinforcement ratio increases, because of the increase of M_{u0}.

As the FRP normalized reinforcement ratio increases, the point of maximum of the curve corresponds to lower values of θ, θ_{min}, and to lower values of H_a, H_{amin}. Figs. 4b–d show how H_{amin} and θ_{min} decrease with increasing ω. From Figs. 4b and c it is evident as small FRP normalized reinforcement ratios can decrease significantly the minimum lateral thrust. For $\omega = 0.10$ (which in this example corresponds to an FRP thickness of 0.12 mm, i.e. one ply) and $\omega = 0.20$ (two plies), H_{amin} is 53% and 67% lower than for the unstrengthened arch, respectively. This implies a significant reduction in the dimensions required to piers, tie-beams or tie-rods.

Fig. 4g shows the line of thrust corresponding to H_{amin} for different values of ω. The dashed lines evidence the location of the point of tangency, θ_{min}, which decreases with increasing ω. It is also clear that, as the eccentricity at the crown section increases, the line of thrust is external to the arch thickness along a larger portion of the arch. Hence, in order for the computed decrease in H_{amin} to be possible, the FRP reinforcement must be extended to cover a minimum angle $2\alpha_{min}$ (indicated by the dash–dot lines) which increases with increasing ω, see Fig. 4e (note that an appropriate anchorage length of the FRP must be provided beyond $2\alpha_{min}$ on both sides). If the FRP reinforcement spans a smaller angle, the minimum thrust is larger

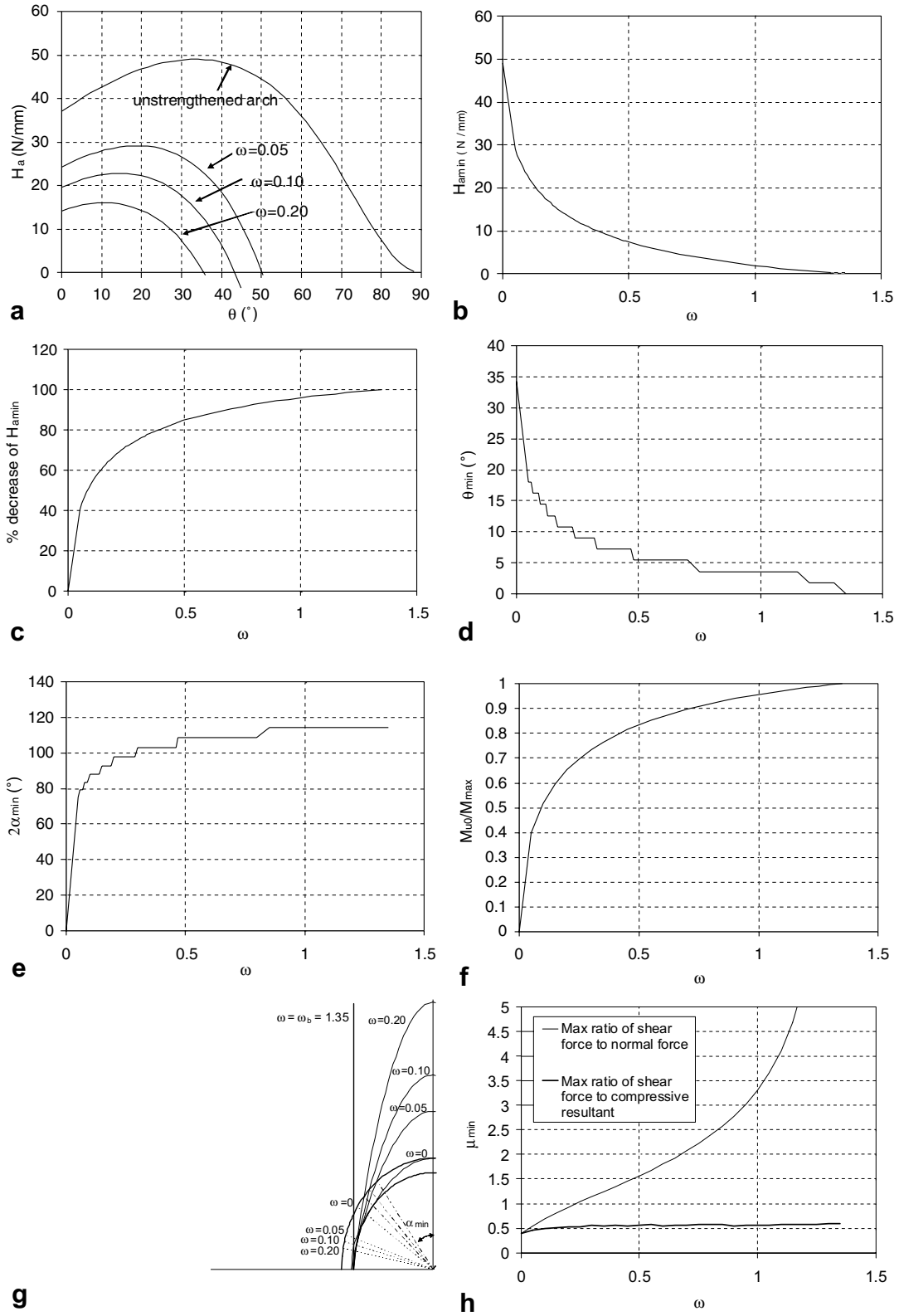

Fig. 4. Example 1. $w = 18{,}000\ \mathrm{N/m^3}$, $q = 5000\ \mathrm{N/m^2}$, $s = 700$ mm, $R = 5$ m, $f_{\mathrm{Mu}} = 1\ \mathrm{N/mm^2}$, $\varepsilon_{\mathrm{Mu}} = 0.003$, $E_{\mathrm{frp}} = 200$ GPa, $\varepsilon_{\mathrm{frpu}} = 0.01$. (a) Lateral thrust H_{a} versus the angle θ of the intrados hinge. (b) Minimum lateral thrust H_{amin} versus FRP normalized reinforcement ratio ω. (c) Percent decrease in H_{amin} versus ω. (d) Angle of the intrados hinge corresponding to H_{amin} versus ω. (e) Minimum angle spanned by the FRP reinforcement corresponding to H_{amin} versus ω. (f) Ratio of ultimate moment of the strengthened cross-section under bending to the maximum moment of external loads, versus ω. (g) Line of thrust corresponding to H_{amin} for the unstrengthened and the strengthened arch. (h) Minimum coefficient of friction corresponding to H_{amin} to prevent failure by sliding of the mortar joints.

than H_{amin} computed previously. It can be calculated by imposing that the line of thrust intersects the extrados of the arch at the radial section corresponding to termination of the reinforcement (excluding the length required for anchorage).

As ω increases, θ_{lim} and θ_{min} both decrease, until they may finally become coincident and equal to zero (as will be shown in Example 2, this is not always the case). The corresponding value of ω is herein termed ω_b. For $\omega = \omega_b$, Eq. (16) becomes as follows:

$$M_{u0} = P_v(0)d_1(0) + Q_v(0)d_2(0) = M_{max} \quad (17)$$

i.e. the ultimate moment of the strengthened cross-section under pure bending equals the maximum moment of the external loads M_{max} (Fig. 4f). In this limit condition, the minimum thrust is equal to zero. The line of thrust is tangent to the intrados at the abutment section and hence degenerates into two vertical lines (Fig. 4g). The arch behaves like a simply supported beam. In this example $\omega_b = 1.35$, corresponding to an FRP thickness of 1.58 mm, i.e. very large for practical purposes using wet lay-up systems.

It can be verified (but is omitted here for brevity) that, once the cross-section at the crown reaches the boundary of the bending moment—normal force domain, the points representative of all the other radial cross-sections fall inside this same boundary. Hence the computed line of thrust is admissible.

As Fig. 4g suggests, the inclination of the line of thrust with respect to the axis of the arch increases with increasing ω, which indicates that sliding of the mortar joints becomes more critical. Fig. 4h shows the minimum coefficient of friction required to avoid sliding failure, μ_{min}, as a function of ω. In an unstrengthened arch, μ_{min} would be taken as the maximum shear force to normal force ratio (in absolute value) in all the cross-sections of the arch. Keeping the same definition for the strengthened arch, μ_{min} would attain very large values (Fig. 4h, thin curve) indicating that a large reinforcement ratio would be underexploited due to sliding failure. In particular, for $\omega = \omega_b$, μ_{min} would tend to infinity. Assuming for masonry $\mu = 0.5$ or $\mu = 0.7$ would yield an optimal ω of about 0.05 or 0.1, respectively. However in a strengthened arch, due to the presence of the tensile force in the FRP, the resultant of the compressive stresses, C, is larger than the normal force N, at least in the cross-sections where the line of thrust lies outside the thickness of the arch (in the other sections, the tensile force in the FRP is either zero or negligible). The resultant C can be reasonably assumed to be responsible for the frictional resistance of the joint instead of the normal force N [9]. This resultant can be computed by making appropriate assumptions on the behavior of the cross-section under compression and bending. Rather than assuming an elastic behavior, which is rather unrealistic due to microcracking, it may be assumed that the compressive stresses are evenly distributed over one third of the height of the cross-section [9]. The curve giving μ_{min} as the maximum shear force to compressive resultant ratio (in absolute value) is reported in Fig. 4h (thick curve). The values of μ_{min} are in this case significantly lower, stabilizing at about 0.55 for large FRP ratios. This indicates that sliding of the mortar joints would not compromise the reduction (or even the elimination) of lateral thrust achievable with the FRP reinforcement, provided that the coefficient of friction of the block-mortar interface is at least 0.55.

2.4.2. Example 2

In this example, all geometry and material parameters are the same of Example 1, while the uniform load q is equal to 10,000 N/m^2. Also in this case, small FRP normalized reinforcement ratios can decrease significantly the minimum lateral thrust (Figs. 5a and b) while θ_{min} decreases and α_{min} increases accordingly (Figs. 5c and d). As ω increases the rate of decrease of the minimum thrust becomes increasingly slow, indicating a reduced effectiveness of large amounts of FRP. For ω equal to 3 (corresponding in this example to an FRP thickness of 3.5 mm, i.e. unrealistically large) all the curves in Fig. 5 have nearly stabilized at a constant value. The ultimate moment of the cross-section M_u does not reach the maximum moment of the external loads M_{max} (Fig. 5e), so that the minimum thrust does not decrease to zero. The minimum coefficient of friction computed as for the unstrengthened arch does not tend to infinity as the line of thrust does not degenerate into vertical lines, but nevertheless attains very large values. However, μ_{min} computed as illustrated above stabilizes at about 0.55 as in the previous example.

This example, compared with the previous one, indicates that the application of the FRP may or may not allow to reach a complete elimination of the minimum lateral thrust of an arch, depending on the relationship between the ultimate moment of a cross-section under pure bending strengthened with a very large amount of FRP (the amount taken as maximum for practical and/or economic reasons) and the maximum moment of the external loads. There may be situations where the former cannot reach the latter, due to the asymptotic trend of the ultimate moment of a strengthened cross-section versus the amount of reinforcement (discussed previously, see Fig. 3c). From the economic standpoint, the best exploitation of the FRP is attained for low values of ω, which may result in large reductions of the minimum thrust as shown in the previous examples.

2.5. Arch strengthened at the extrados

A reduction in the minimum lateral thrust can be also obtained by strengthening the arch at the extrados. In this case, the FRP must span an angle starting from the abutments towards the haunches, hence the line of thrust can fall outside the arch thickness in the internal part of the

intrados. The computation can be conducted in analogy to the one illustrated above, and is not reported for brevity. Note that in this case the FRP must be properly anchored at the abutments. If the FRP reinforcement ratio is such that the ultimate moment of the cross-section at the abutment equals the maximum moment of the external loads, the minimum thrust becomes zero and the arch behaves like two cantilever beams of length R. This theoretical limit condition may not be reached in practice for the reasons discussed above.

3. Minimum lateral thrust of masonry edge vaults

3.1. Morphology of edge vaults

The theoretical analysis outlined above is herein applied to masonry edge vaults, a typology of masonry vaults typical of some regions of Italy. Edge vaults are structurally similar to cross-vaults. They are constituted by four barrel webs, whose vertex points do not meet at the crown of the vault as in the cross-vault (point O in Fig. 6a) but are

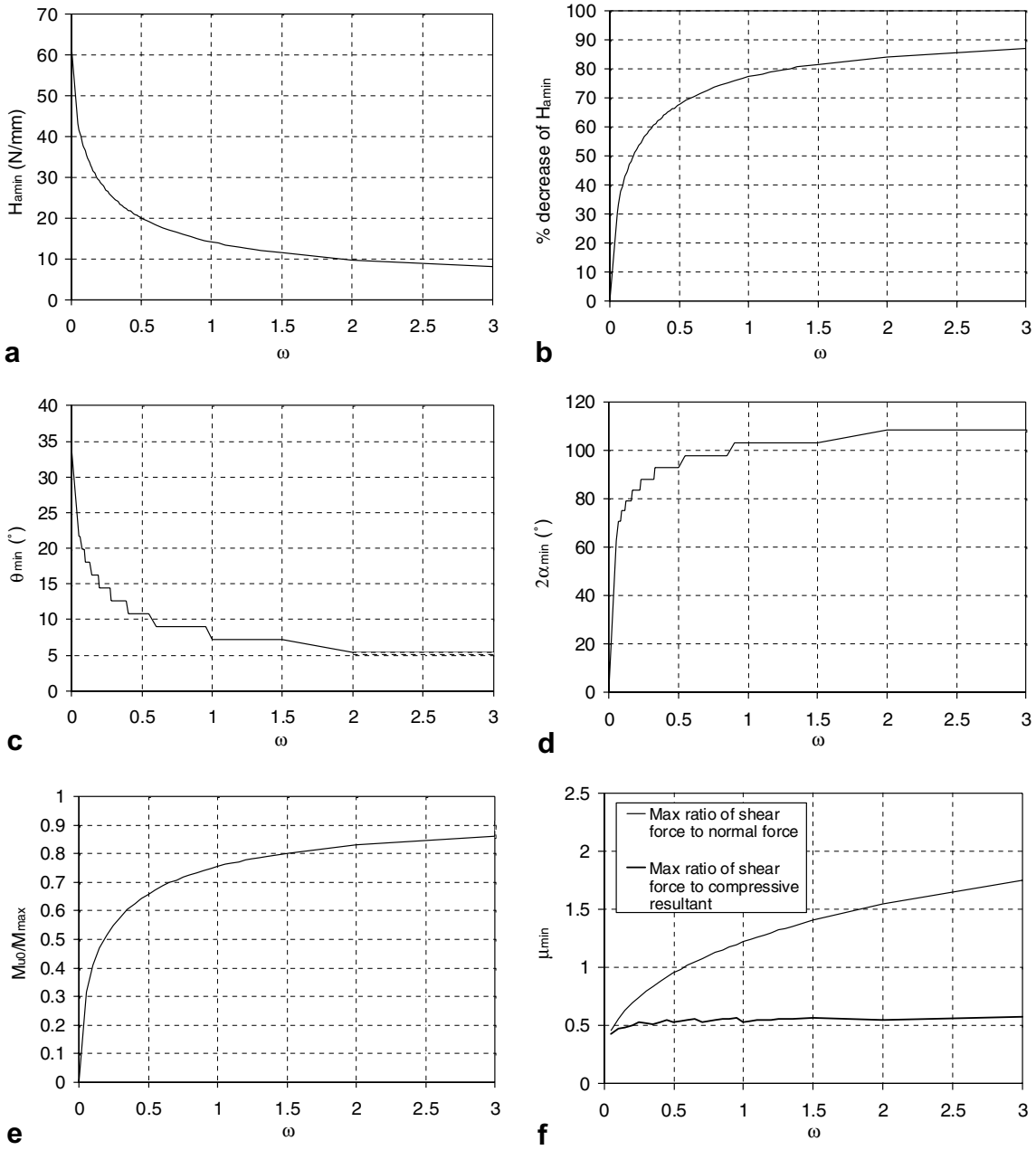

Fig. 5. Example 2. $w = 18{,}000$ N/m^3, $q = 10{,}000$ N/m^2, $s = 700$ mm, $R = 5$ m, $f_{Mu} = 1$ N/mm^2, $\varepsilon_{Mu} = 0.003$. (a) Minimum lateral thrust H_{amin} versus FRP normalized reinforcement ratio ω. (b) Percent decrease in H_{amin} versus ω. (c) Angle of the intrados hinge corresponding to H_{amin} versus ω. (d) Minimum angle spanned by the FRP reinforcement corresponding to H_{amin} versus ω. (e) Ratio of ultimate moment of the strengthened cross-section under bending to the maximum moment of external loads, versus ω. (f) Minimum coefficient of friction corresponding to H_{amin} to prevent failure by sliding of the mortar joints.

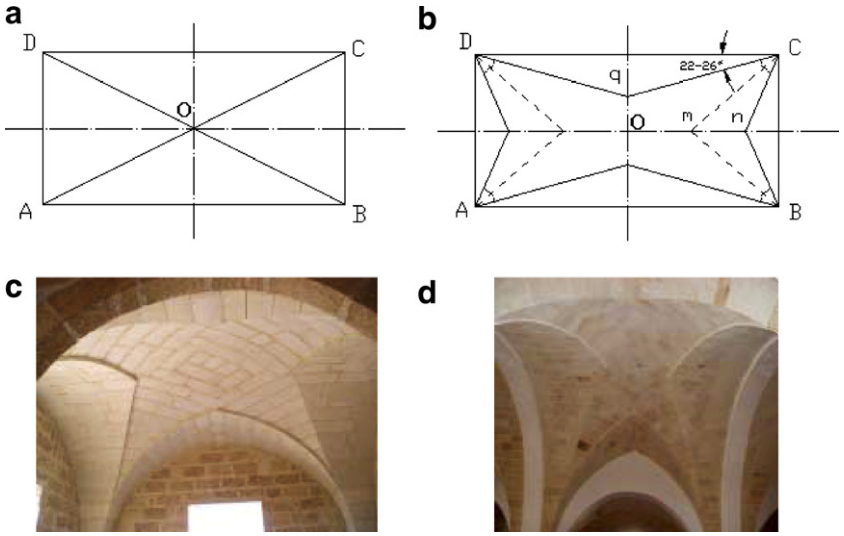

Fig. 6. Geometry of edge vaults. (a) Plan of a cross-vault. (b) Plan of an edge vault. (c) An example of edge vault over square plan with semicircular webs. (d) An example of edge vault over rectangular plan with semicircular (long sides) and pointed (short sides) webs.

moved backwards, leaving in the middle an empty space covered with a double-curvature shell portion (Fig. 6b). This central shell has the shape of a four-point star, and for this reason the edge vault is also commonly termed "star vault". The boundary edges between the barrel webs and the central shell for the long and for the short side of a rectangular plan (e.g. edges Cq for the long side and Cn for the short side in Fig. 6b) are symmetric with respect to the bisecting lines of the 90-degree angles between the sides of the plan (i.e. in Fig. 6b, Cq and Cn are symmetric with respect to the bisecting line Cm of the 90-degree angle $B\hat{C}D$). The angle formed by these boundary edges with the corresponding sides (e.g. $q\hat{C}D = n\hat{C}B$ in Fig. 6b) is equal to 22 or 26° when the width of the voussoirs equals 200 or 250 mm, respectively [6].

For vaults with rectangular plan, the shape of the directrix of the webs is usually semicircular, elliptical or pointed for the webs of the two long sides, and pointed (less commonly semicircular) for the webs of the two short sides, whereas vaults over square plans frequently have semicircular directrix for all four webs (Figs. 6c and d). The heights of the vault key and of the keys of the barrel webs differ by a small amount, known as *sovrassesto*. The initial portions of the webs (i.e. those that, for each web, encompass an angle of about 30° starting from the springers on both sides) are similar to those of the cross-vault with the same directrix, hence the edges of the webs coincide in plan with the bisectors of the angles (segment MP in Fig. 7a). In local technical dialect these portions are called *appese*, this term will be translated as *abutments* as follows. The portions of the webs supported by the abutments are herein considered as the four lateral arches of the vault, reflecting the fact that these portions transmit the lateral thrust from the vaults to the piers. Fig. 6c also shows the pattern of the ashlars, which typically follows the French system in the webs and a spiral configuration in the central shell.

Edge vaults are typically made of calcarenite tuff or similar locally available varieties of stone, and the ashlars are assembled with thin mortar joints. More details about history, geometry and construction of these vaults are available elsewhere [6,15]. It is worth noting that edge vaults are similar in appearance to the better known Gothic stellar vaults. However, the structural behaviour of the two types of vaults is significantly different [6].

3.2. Analytical definition of the mid-plane surface

In accordance with the characteristics of the tested vault, reference is made herein to a vault with square plan and webs of semicircular directrix with radius a. It is also assumed that the edges of the webs form a 22-degree angle with the respective sides of the plan (but computation for the case of a 26-degree angle is perfectly analogous).

The origin of the coordinate system is taken coincident with the center of symmetry of the plan on the springer plane, the x and y axes are taken coincident with the axes of symmetry of the plan and the z axis is orthogonal to them and directed upwards (Fig. 7). The double symmetry allows only a quarter of the vault to be defined. The mid-plane of the central star-shaped shell can be considered part of an ellipsoidal surface whose equatorial ellipse is circumscribed to the plan of the ambient to be covered. The equation is

$$z_c(x,y) = f \cdot \sqrt{1 - \left(\frac{x^2 + y^2}{\beta^2}\right)} \tag{18}$$

where z_c is the z coordinate of the generic point of the middle plane of the shell, f is the height of the vault key to the x–y plane, and β is a coefficient that can be determined by enforcing point M of coordinates (a $\cos 30°$, a $\cos 30°$, a $\sin 30°$) to belong to the shell surface:

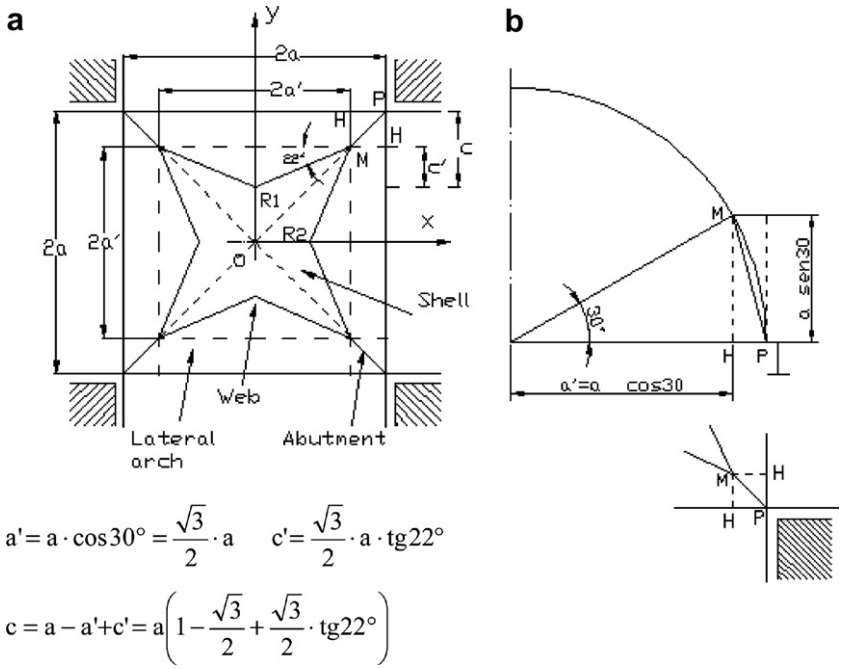

$$a' = a \cdot \cos 30^\circ = \frac{\sqrt{3}}{2} \cdot a \qquad c' = \frac{\sqrt{3}}{2} \cdot a \cdot \mathrm{tg}22^\circ$$

$$c = a - a' + c' = a\left(1 - \frac{\sqrt{3}}{2} + \frac{\sqrt{3}}{2} \cdot \mathrm{tg}22^\circ\right)$$

Fig. 7. (a) Plan of the vault. (b) Barrel web section in the connection with the lateral arch.

$$\beta = \sqrt{\frac{6a^2 f^2}{4f^2 - a^2}} \tag{19}$$

Moreover, by enforcing point R_1 of coordinates (0, a–c, a) to belong to the shell surface, the following relationship is obtained between the height of the vault key and the height of the keys of the four lateral arches:

$$\frac{f}{a} = 1.08 \tag{20}$$

which is in sufficiently good agreement with the f/a ratios typically adopted in the construction practice. Finally, the equation of the web directrix can be obtained by combining the equation of the shell mid-plane (Eq. (18)) and that of the vertical plane for M and R_1:

$$y = (a' - c') + \frac{c'}{a'}x \tag{21}$$

where a' and c' are indicated in Fig. 7. The result is as follows:

$$z_u(x) = f \cdot \sqrt{1 - \frac{x^2 + \left[(a' - c') + \frac{c'}{a'}x\right]^2}{\beta^2}} \tag{22}$$

Eq. (22), referred to half of the web directrix, generates a slightly pointed directrix, with a maximum deviation from the semicircular shape of about 3%. Alternatively, if the web directrix is given a semicircular shape, the intersection between the middle shell and each web is no longer a plane but rather a curved surface, whose trace on the x–y plane is no longer segment MR_1 but a curve between the same points. Considering the variety of shapes of the web directrix and the unavoidable differences between constructed and analytical geometries, the equations given above are sufficiently accurate for practical purposes. An analogous consideration holds for the further approximations that have been implicitly adopted thus far, such as considering the vault thickness significantly smaller than its plan dimensions, and neglecting small details of the construction practice such as, for instance, the 3–4 cm difference of thickness between central shell and webs (traditionally adopted for aesthetic reasons, see Fig. 6c) or the slight slope of the key line of the web upwards from the lateral arch to the vertex.

3.3. Computation of the minimum lateral thrust

For a simplified computation of the lateral thrust transmitted from the vault to the piers, the loads acting on the vault are computed and appropriately distributed on the four lateral arches according to the respective "influence widths". In turn, the lateral arches are analyzed as illustrated in the previous section, with the exception that the uniform load q acting on the arch (excluding its self weight) is substituted by a function $q(x)$. In accordance with the characteristics of the tested vault, the vault extrados is considered filled with inert material to the level of the vault key. The load acting on each of the four lateral arches is then the sum of: self weight of the arch itself and of its spandrel fill; self weight of the portion of web and central shell "pertaining" to the arch and of the relative fill; uniformly distributed load applied on the extrados of the vault in the region which "pertains" to the arch. The mentioned load components can be easily computed analytically based on the previous definition of the vault mid-plane surface. Once $q(x)$ is computed, Q_v and d_2 (previously given by Eq. (14)) are expressed as follows:

$$Q_v = \int_0^{R_e \cos\theta} q(x)\mathrm{d}x \quad d_2 = R_i \cos\theta - \frac{\int_0^{R_e \cos\theta} q(x)x\mathrm{d}x}{\int_0^{R_e \cos\theta} q(x)\mathrm{d}x} \tag{23a-b}$$

whereas P_v and d_1 are always given by Eq. (13).

3.4. Test program

Two tests were carried out to evaluate the effectiveness of FRP strengthening at the intrados to reduce the lateral thrust of the vault. The tests were conducted on a masonry edge vault with square plan and semicircular directrix of the barrel webs, whose dimensions are illustrated in Fig. 8. These dimensions are assumed to be half the dimensions of the "real" vault, of which the one subjected to test is the scaled prototype. This 1:2 scale was used to determine the dimensions of the single voussoirs, in accordance with the traditional geometric rules of the edge vault construction. The thickness of the four webs and of the central shell was equal to 90 mm. Spandrel fill made of tuff was located on the vault so as to obtain a flat top surface at the level of the crown, on which the external uniform load could be applied.

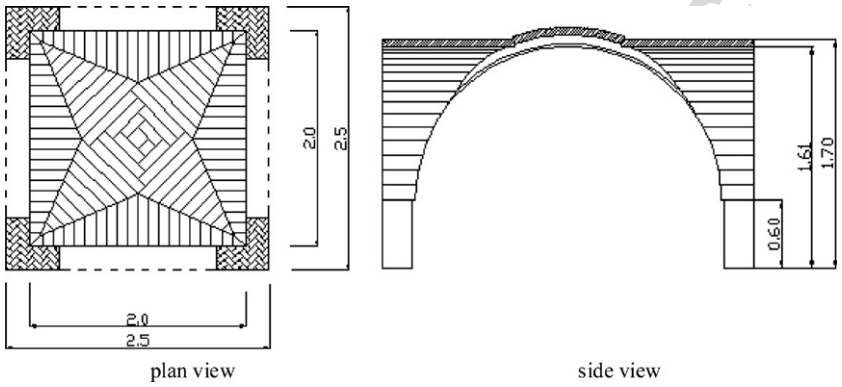

Fig. 8. Scaled masonry vaults subjected to testing (dimensions in m).

Table 1
Material properties

Measured property	Specimen geometry	No. of specimens	UNI (Italian national) standard	Average value (N/mm^2)	Coefficient of variation (%)
Stone					
Compressive strength	Cubes, 70-mm edge	10	9724–3	1.81	10.2
Bending tensile strength	Prisms, 30 × 20 × 120 mm, 100-mm net span	5	9724-5	0.93	5.5
Compressive elastic modulus	Prisms, 50 × 50 × 200 mm	4	9724-8	392.9	4.9
Mortar					
Compressive strength	Prisms, 40 × 40 × 80 mm	16	EN 196-1	0.55	14.4
Bending tensile strength	Prisms, 40 × 40 × 160 mm, 100-mm net span	8	EN 196-1	0.30	16.8
Compressive elastic modulus	Prisms, 40 × 40 × 160 mm	9	EN 196-1	78.8	31

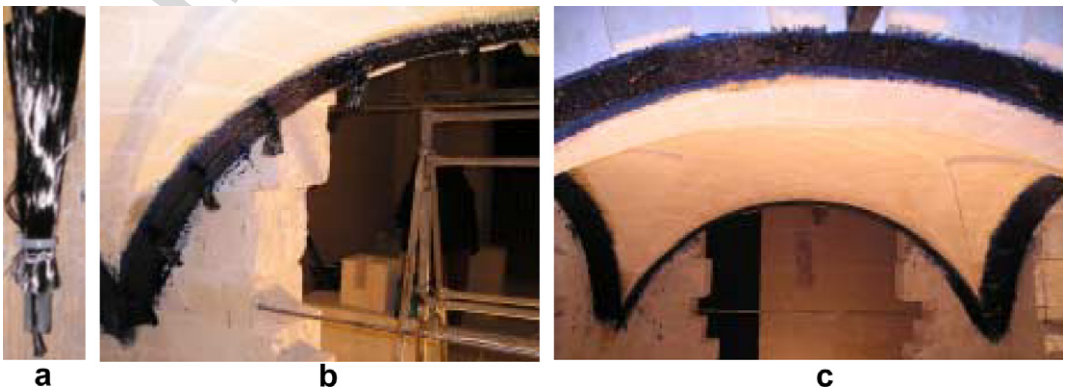

Fig. 9. Strengthening of the vaults with FRP sheet. (a) FRP spike; (b) the spikes are inserted through the sheet into the holes; (c) picture of the vault after completion of strengthening.

The tests reported were both conducted on the same vault. First, the unstrengthened vault was tested under uniform loading, measuring the lateral thrust by means of four steel tie-rods (as better detailed in following sections). The vault was then unloaded and strengthened with FRP sheets, as described in a following section. A second test, under the same uniform loading of the first test, was conducted on the strengthened vault, again measuring the lateral thrust absorbed by the tie-rods.

3.5. Material properties

The ashlars were made of a type of local calcarenite tuff, on which characterization tests were performed to

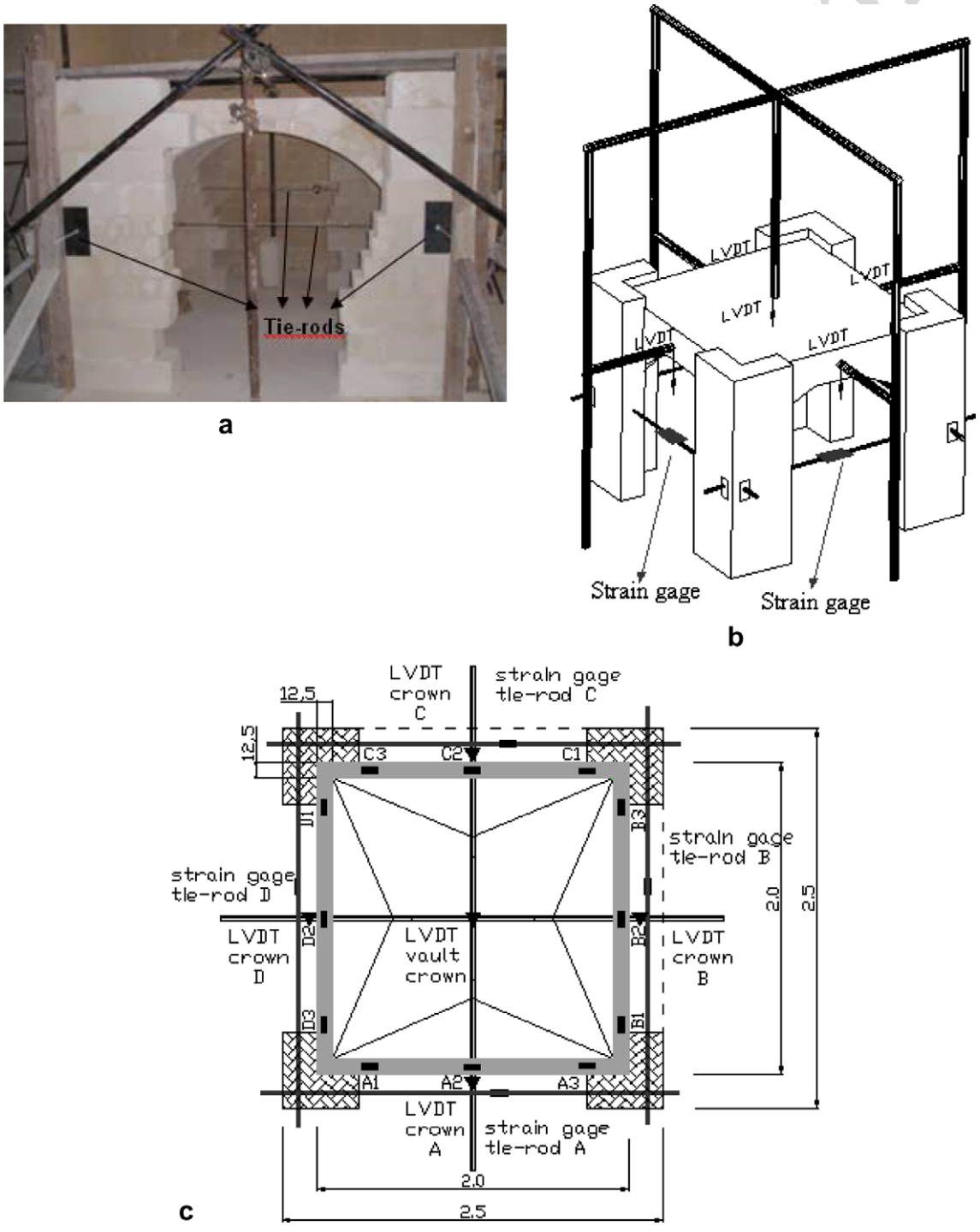

Fig. 10. Test setup and instrumentation. (a) Unstrengthened vault with steel tie-rods, temporary wooden buttresses and frame of steel tubes used to fix the LVDTs. (b) Scheme of the instrumentation on the unstrengthened vault. (c) Strengthened vault with strain gages on the FRP sheet at various locations.

measure compressive strength, compressive modulus of elasticity, and bending tensile strength. This particular type of tuff, upon visual observation, shows no distinguishable planes of sedimentation. Hence it was assumed that the plane of sedimentation would exert no appreciable influence on the material properties. This was confirmed by the low scatter observed in test results. The mortar used for the joints was made of lime and tuff sand. Characterization tests were performed to measure its compressive strength and bending tensile strength. For both tuff and mortar, the specimen number and geometry and the test results are reported in Table 1. The carbon FRP (CFRP) unidirectional sheet used for strengthening of the vault had an average tensile strength of 3846 MPa and an average tensile modulus of elasticity of 233.7 GPa, as obtained from previous characterization tests. The nominal thickness of one ply (referred to the fibers only) was 0.165 mm.

3.6. Specimen preparation

After the first test, the vault was strengthened with one ply of FRP at the intrados of the four lateral arches, spanning an angle 2α of about 150°. Application of the sheets followed the usual steps of the wet lay-up technique, with the only addition that FRP spikes were used to prevent debonding of the sheets from the masonry substrate. As well known, application of the reinforcement at the intrados makes debonding particularly critical. In this case, equilibrium dictates that the shear bond stresses between FRP and masonry are accompanied by normal tensile stresses, which accelerate debonding failure [10,18]. Previous researchers proposed the use of FRP spikes to enhance bond to curved substrates [8] and proved its effectiveness [8,1].

In this program, each spike was made of a 50-mm piece of CFRP sand-coated bar with 8-mm diameter, mechanically connected to a bundle of 100-mm long dry carbon fibers (Fig. 9a). Installation of the spikes was carried out as follows. First, holes were drilled into the masonry substrate to a depth slightly larger than the length of the CFRP bar pieces. The holes were positioned on alternate voussoirs where the FRP had to be bonded, starting from the last voussoir of the abutment, for a total of 12 holes per lateral arch. The holes were cleaned with pressurized air. The bond surface, including the holes, was primed, then the first layer of saturant was applied on the masonry surface and the same saturant was used to partially fill the holes. The FRP sheet and the second layer of saturant were applied next. At the location of each hole, the bar extremity of the FRP spike was inserted through the sheet into the hole by locally enlarging the unidirectional fibers of the sheet (Fig. 9b). The fiber bundle was then spread in circular fashion, folded and pressed over the CFRP sheet, and impregnated with a layer of saturant (Fig. 9c). The strengthened vault was tested three days after the application of the FRP.

3.7. Instrumentation and test procedure

The lateral thrust of the vault was measured by means of four steel tie-rods with 10-mm diameter, applied on the four lateral arches at a height corresponding to about 30° from the springers. Each rod had a smooth surface and was threaded at the ends to react the force against the external surfaces of the piers with a screw nut, a washer and a reaction plate.

The unstrengthened vault was instrumented with five LVDTs, measuring the vertical displacements of the crowns of the four lateral arches and of the vault crown, and four strain gages, measuring the strains of the four tie-rods from which the lateral thrusts of the four lateral arches could be computed. The strengthened vault was also instrumented with twelve additional strain gages, three per lateral arch, applied on the FRP sheet parallel to the fiber direction. The three strain gages on each arch were located at approximately 50° from the horizontal on both sides, and at the crown. Fig. 10 illustrates the instrumentation setup. A uniform load was applied on the extrados of the vault by means of manually positioned sand bags. The load was applied in three steps, corresponding to 200, 400 and 562.5 kgf/m^2, respectively, for a total load of 2250 kgf on the entire vault at the final step.

3.8. Test results

Figs. 11a and b show the vertical displacement of the crown of three of the four lateral arches (displacement data from the crown of arch A was lost due to malfunctioning of the LVDT) and of the vault crown for the unstrengthened and the strengthened vaults, respectively. In Fig. 11a, the first vertical line in the graph marks the removal of the temporary wooden buttresses, used to react the thrust of the vault prior to installation of the tie-rods. In Fig. 11b, the vertical line at time = 0 corresponds to starting of the test. In both figures, the subsequent vertical lines mark the instants at which one, two and three layers of bags are laid on the top surface of the vault and the applied load is correspondingly 200, 400 and 562.5 kgf/m^2. The unloading steps are also indicated. In both figures, the displacement of the vault crown is about twice the average displacement of the crown of the lateral arches, and they both increase as the applied load increases and decrease during unloading. A comparison of the two figures shows a notable reduction of the measured displacements as a result of application of the FRP. For the unstrengthened vault, a residual displacement is noted when the applied load is removed, due to settling phenomena in the mortar joints and in the piers. Such phenomenon is not relevant in the strengthened vault.

Figs. 12a and b illustrate the lateral thrusts absorbed by the tie-rods on the lateral arches of the unstrengthened and strengthened vaults, respectively (one of the four strain gages did not function properly). In both figures, the lateral thrusts increase as the applied load increases, and decrease during unloading. Fig. 12a shows as the thrusts build up

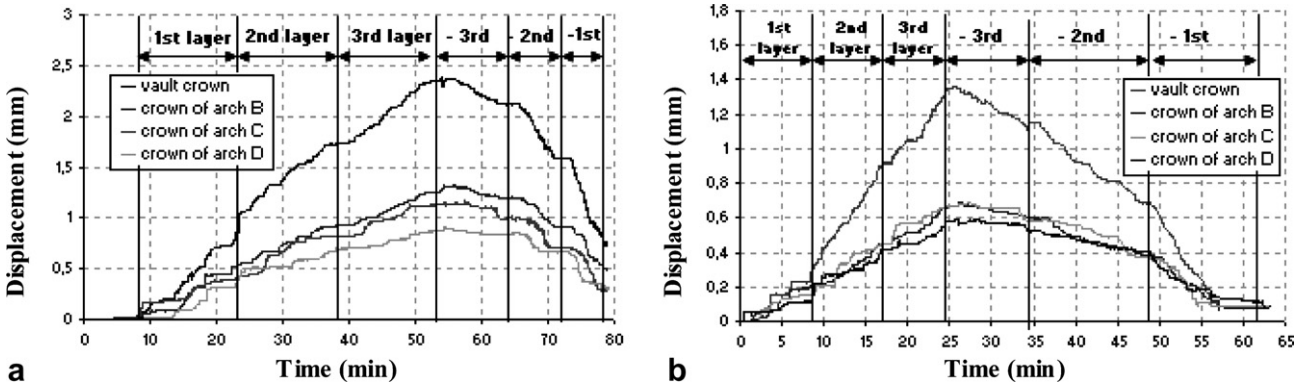

Fig. 11. Displacements of the arch crowns and of the vault crown vs. time for the unstrengthened (a) and strengthened (b) vaults.

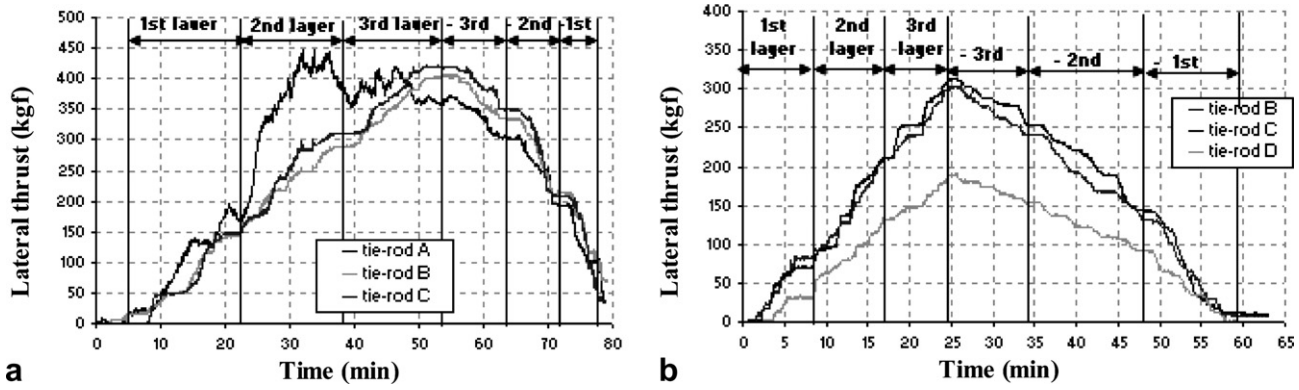

Fig. 12. Lateral thrusts on the tie-rods vs. time for the unstrengthened (a) and strengthened (b) vaults.

already at the removal of the wooden buttresses, due to partial transfer to the tie-rods of the thrust generated by self weight and spandrel fill. The remaining portion is absorbed by the piers at least in the initial phase. A comparison of the two figures shows a notable reduction of the measured thrusts as a result of application of the FRP. The reduction in lateral thrust as a result of FRP strengthening results equal to 62%, 44% and 32% after the first, second, and third step of loading, respectively. This demonstrates as the application of FRP at the intrados produces significant adjustments of the line of thrust, yielding a notable reduction in the lateral thrust transmitted to the piers.

Finally, Figs. 13a and b illustrate the axial load deduced from the strains measured on the FRP sheet at the haunches and at the crowns of the lateral arches, respectively. The axial load in the FRP is compressive at the haunches and tensile at the crown. The compressive strains are characterized by a large scatter, probably due to irregularities caused by local fiber buckling. Conversely, the ten-

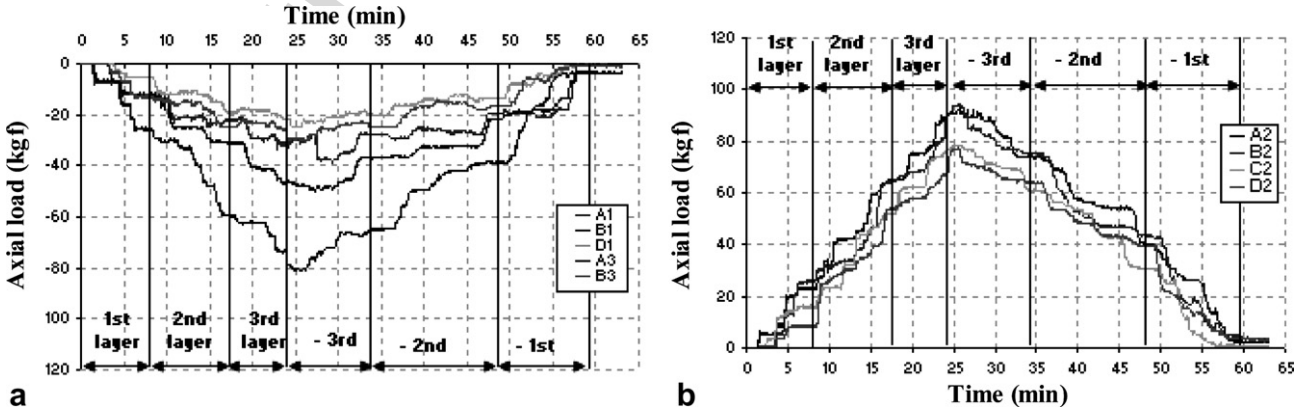

Fig. 13. Axial load in the FRP at the haunches (a) and at the crown (b) of the lateral arches, vs. time.

Table 2
Experimental and theoretical values of the lateral thrust

Loading step (kgf/m^2)	Experimental lateral thrust (kgf)			Theoretical minimum lateral thrust (kgf)		
	Unstrengthened vault[a]	Strengthened vault[a]	Percent reduction (%)	Unstrengthened vault	Strengthened vault	Percent reduction (%)
First step (200)	162	61	62	176	64	63
Second step (400)	330	186	44	277	159	43
Third step (562.5)	398	269	32	359	244	32

[a] Average of three functioning strain gages.

sile strains are reasonably close on all the four lateral arches.

It is worth noting that no visually detectable cracks in the vault and no sign of debonding between the FRP sheet and the masonry substrate were observed during the test.

4. Comparison with theoretical predictions

The theoretical values of the minimum thrust under the three steps of loading were computed as previously illustrated. In the tested vault, the measured unit weight of the tuff was 1428 kgf/m^3, and the same value was assumed for the unit weight of the fill which was made of the same material. The compressive strength of masonry was taken equal to that of the tuff material, considering that in the lateral arches the presence of the mortar joints is believed to exert no appreciable influence on the masonry strength.

Table 2 shows the comparison between the experimental thrust (obtained as the average of the measurements on the four arches) and the theoretical minimum thrust. It can be noted that the measured values of the thrust are always (except in one case) slightly larger than the theoretical values. This was expected because the theoretical analysis delivers the minimum possible thrust. However, the difference between experimental and theoretical values is very limited, demonstrating that the simple illustrated procedure yields accurate predictions of the actual thrusts for both unstrengthened and strengthened vaults. In particular, the effect of the FRP strengthening on the reduction of the thrust is fully captured.

5. Conclusions

Based on the theoretical and experimental study reported above, the following conclusions can be drawn:

- The application of FRP reinforcement to a masonry arch allows a substantial reduction of the lateral thrust transmitted to the piers. The FRP reinforcement should be placed either at the intrados spanning an angle centered at the crown, or at the extrados spanning two angles from the abutments towards the haunches (and anchored at the abutments).
- The complete elimination of the thrust is possible when the amount of reinforcement is such that the ultimate moment of the strengthened masonry cross-section under pure bending equals the maximum moment of the external load. In this condition, the arch behaves like a beam. The amount of reduction of the minimum thrust may be limited by the insufficient extension of the reinforcement or by the possibility of sliding of the mortar joints.
- Strengthening the four lateral arches of an edge vault with FRP sheet at the intrados produces a significant reduction of the thrust transmitted to the piers.
- The use of FRP anchor spikes is effective in preventing debonding of an FRP sheet applied at the intrados of a masonry arch. The application of FRP at the intrados can then be regarded as an effective solution. In many cases, strengthening of a vault at the extrados is unfeasible or significantly onerous, as it implies removal of floor finishes and spandrel fill.
- The simple model illustrated in the paper can be used to evaluate with satisfactory accuracy the reduction of thrust obtained by the use of the FRP, and can then be considered a useful design tool.

Acknowledgement

The authors wish to acknowledge Mr. Giampiero and Mr. Piero Montalbano of Real Property (Manduria, Ta, Italy), for providing the site instrumentation and making the experiments possible, Mr. Giuseppe Ruggieri for constructing the scaled prototypes of edge vault, and MAC Italia S.p.A. for providing the FRP system free of charge.

References

[1] Aiello MA, De Lorenzis L, Galati N, La Tegola A. Bond between FRP laminates and curved concrete substrates with anchoring composite spikes. In: Proceedings IMTCR'04, Lecce, Italy; 2004.
[2] Blasi C, Foraboschi P. The masonry arch: a continuum approach and a discrete approach. Special issue of international journal from computational mechanics publications 1990;6(2):68–74.
[3] Blasi C, Foraboschi P. Analytical approach to collapse mechanisms of circular masonry arch. J Struct Eng 1994;120(8):2288–309.
[4] Briccoli Bati S, Rovero L, Tonietti U. Strengthening of masonry arches with composite materials. In: Proceedings IMTCR04, Lecce, Italy; 2004. p. 386–402.
[5] Chen JF. Load-bearing capacity of masonry arch bridges strengthened with fibre reinforced polymer composites. Adv Struct Eng 2002;5(1).

[6] Colaianni VG. Le volte leccesi. Dedalo libri ed., Bari, 1967 [in Italian].
[7] Como M, Ianniruberto U, Imbimbo M. On the structural capacity of masonry arches strengthened by FRP. In: Proceedings of the third international conference on arch bridges, Paris, September 2001.
[8] Eshwar N, Ibell T, Nanni A. CFRP strengthening of concrete bridges with curved soffits. In: Proc structural faults + Repair 2003, London, UK. MC Forde, Ed., CD-ROM, 2003, 10pp.
[9] Faccio P, Foraboschi P. Volte a botte ed archi, L'Edilizia, De Lettera Ed., Milano, 5/6, 2000. p. 48–56 [in Italian].
[10] Foraboschi P. Strengthening of masonry arches with fiber-reinforced polymer strips. ASCE J Compos Construct 2004;8(3).
[11] Heyman J. The masonry arch. West Sussex, UK: Ellis Horwood-Wiley; 1982.
[12] Ianniruberto U, Rinaldi Z. Resistenza laterale di portali in muratura rinforzati con FRP all'intradosso. In: Proceedings of the XI National Conference ANIDIS 04, Genova, Italy, 2004 [in Italian].
[13] ICOMOS. International Scientific Committee for Analysis and Restoration of Structures of Architectural Heritage, Recommendations for the analysis, conservation and structural restoration of architectural heritage, Parigi, 2001.
[14] Italian National Research Council (CNR). "Istruzioni per la Progettazione, l'Esecuzione ed il Controllo di Interventi di Consolidamento Statico mediante l'utilizzo di Compositi Fibrorinforzati—Materiali, strutture di c.a. e di c.a.p., strutture murarie", CNR-DT 200/2004, Italy, 2004 [in Italian, translation into English underway].
[15] Pecoraro I. I sistemi voltati nel Salento fra XVI e XVIII secolo: origini, geometria costruttiva e problemi di conservazione. PhD thesis, University of Rome, 2002 [in Italian].
[16] Triantafillou TC. Strengthening of masonry structures using epoxy-bonded FRP laminates. J Compos for Construct, ASCE 1998;2(2):96–104.
[17] Triantafillou TC. Strengthening of masonry structures using epoxy-bonded FRP laminates Errata. J Compos for Construct, ASCE 1998;2(4):203.
[18] Valluzzi MR, Valdemarca M, Modena C. Behavior of brick masonry vaults strengthened by FRP Laminates. J Compos Construct 2001;5(3):163–9.